NASA TECHNICAL MEMORANDUM

N79-31206

NASA TM-75430

INVESTIGATION OF AIR STREAM FROM COMBUSTOR-LINER AIR ENTRY HOLES, III

Tetsuro Aiba and Tokuji Nakano

Translation of "Kō fuka nenshōki no kūkikō kara no nagare ni tsuite (III)", National Aerospace Lab., Tokyo (Japan), Report No. NAL-TR-369, 1974, pp. 1-23.

NATIONAL AERONAUTICS AND SPACE ADMINISTRATION
WASHINGTON, D. C. 20546 AUGUST 1979

STANDARD TITLE PAGE

1. Report No. NASA TM-75430	2. Government Accession No.	3. Recipient's Catalog No.
4. Title and Subtitle: INVESTIGATION OF AIR STREAM FROM COMBUSTOR-LINER AIR ENTRY HOLES, III		5. Report Date: AUGUST 1979 6. Performing Organization Code
7. Author(s): Tetsuro Aiba and Tokuji Nakano		8. Performing Organization Report No. 10. Work Unit No.
9. Performing Organization Name and Address: SCITRAN, Box 5456, Santa Barbara, CA 93108		11. Contract or Grant No. NASW-3198 13. Type of Report and Period Covered: Translation
12. Sponsoring Agency Name and Address: National Aeronautics and Space Administration, Washington, D.C. 20546		14. Sponsoring Agency Code

15. Supplementary Notes

Translation of "Kō fuka nenshōki no kūkikō kara no nagare ni tsuite (III)", National Aerospace Lab., Tokyo (Japan), Report No. NAL-TR-369, 1974, pp. 1-23.

16. Abstract: Jets flowing from air entry holes of the combustor-liner of a gas turbine were investigated following previous experiments using simplified models. Cold air was supplied through the air entry holes into the primary hot-gas flows. The mass flow of the primary hot-gas and issuing jets was measured, and the behavior of the air jets was studied by the measurement of the temperature distribution of the gas mixture. The air-jets flowing from three circular air entry holes parallel to the primary flow, single streamwise-long holes, and two opposing circular holes were studied along with the effects of jet and gas stream velocities, and of gas temperature. The discharge coefficient, the maximum penetration of the jets, the jet flow path, the mixing of the jets, and temperature distribution across the jets were investigated. Empirical expressions which describe the characteristics of the jets under the conditions of the experiments were formulated. The experimental results are compared with the results given by a standard circular hole and their characteristics are discussed.

17. Key Words (Selected by Author(s))	18. Distribution Statement: Unclassified - Unlimited		
19. Security Classif. (of this report): Unclassified	20. Security Classif. (of this page): Unclassified	21. No. of Pages: 37	22.

NASA-HQ

INVESTIGATION OF AIR STREAM FROM COMBUSTOR-LINER AIR ENTRY HOLES (III)*

Tetsuro Aiba** and Tokuji Nakano**

Abstract /1***

Investigation of the jets flowing from air entry holes of the combustor-liner of a gas turbine was carried out following the previous experiments using simplified models. Cold air was supplied through the air entry holes normally into the primary hot-gas flows. The mass flow of the primary hot-gas and issuing jets were measured, and the behavior of the air-jets was studied by the measurement of the temperature distribution of the gas mixture.

The air-jets flowing from three circular air entry holes being parallel to the primary flow, single streamwise-long holes and two opposing circular holes were studied. The effects of jet and gas stream velocities and of gas temperature, together with these different configurations, were investigated. The discharge coefficient, the maximum penetration of the jets, the jet flow path, the mixing of the jets, and temperature distribution across the jets were investigated. Empirical expressions which describe the characteristics of the jets under the conditions of the experiments were formulated. The experimental results were compared with the results given by a standard circular hole and their characteristics were discussed.

1. Preface

High temperatures and high compressions are required more and more for the operation of the aviation gas turbine combustor

*Received on March 9, 1974

**Department of Motors

***Numbers in margin indicate pagination in original foreign text

and the combustion load factor also has become high. For a high load combustion, the air stream flow inside the combustor has considerable influence on the combustion efficiency, the stability limits of the flame, the temperature distribution at the exit holes of the combustor-liner. In recent years, accurate information on the exhaust gas air stream has been obtained. The poisonous components in the exhaust gas such as CO and NO_x are related to the composition distribution and temperature distribution of the air stream in the combustor, together with the path of "the mass flow of the air stream" and the duration of "stay". The air stream in the combustor is determined mainly by the combustor-liner, the amount swallowed and the individual shape of the liner air entry holes. This report gives results of experiments on flow motions in air stream from the air entry holes of the combustor-liner, the penetrating power of the jets and the jet mixing.

This report is a sequel to the previous reports [1, 2] and discusses supplementary experiments using a model of the air entry holes which are very close to the actual case. Three kinds of the combustor-line air entry holes are used: 1) three round holes were arranged in a straight line on the bottom of the test section, 2) only one elongated hole on the bottom, and 3) round holes on the top and the bottom facing each other in pairs. The three holes in a straight line represent a continuation of the experiment with the single round hole and the two holes reported previously. The elongated hole simulates the shape of the hole commonly used for the dilution air entry hole. The round hole-pairs inside and outside the actual combustor-liner face each other. In this experiment, the main flow was heated and at normal temperature flowed in directly intersecting the heated main flow through the air entry holes built into the test section. The penetrating power of the intersecting jet flows and the mixing of the jets were obtained from the measurements of the temperature distribution at the location of the flow. There are many air

entry holes in the liner of the gas turbine combustor. The measurements of the flows from multiple holes and the elongated hole of this experiment are conducted under conditions closer to the actual conditions, compared with previous measurements restricted to single round holes and only the main flow. All the measurements on the mixing of jets from multiple holes, on the change in the cross-section of the jets from elongated holes, on the penetrating power of each jet and on the mixing of jets gave results different from the previous measurements with certain characteristic features. For this report, which is a supplement to the results of the single round hole experiment, the path of the jet center has been rearranged since the previous report and comparisons with other experiments are also made. /2

2. Experiment Equipment and Methods

The "water jar" shaped combustor at the test facilities in the Department of Motors, National Aerospace Laboratory, was used for this experiment. Figure 1 shows the schematic of this facility. The volume of air that can be used in this facility is 0 - 1.25 kg/s and the air temperature at the exit hole of the radiator can vary between 20 - 40 °C. The "preliminary" combustor can bring the temperature of the main flow up to 600 °C maximum. The fuel used for the preliminary combustor was JP - 4. The inside diameter of the rectifier was 600 mm and converts to a square flow path of 130 mm x 130 mm in the test section. The exit hole at the test section was open to the atmosphere and the total length of the test section was 520 mm. Figure 2 shows pairs of round, air-entry holes, one each on the top and the bottom of the test section. In order to measure the temperature distribution in the flow, a thermocouple was inserted through a small hole on the top of the test section for the three-holes-in-a-straight-line case and for the elongated-hole case. In the case of facing hole pairs, the thermocouple was inserted from the side downstream. Measurements of the compression and the temperature were made at the points shown in Figure 3.

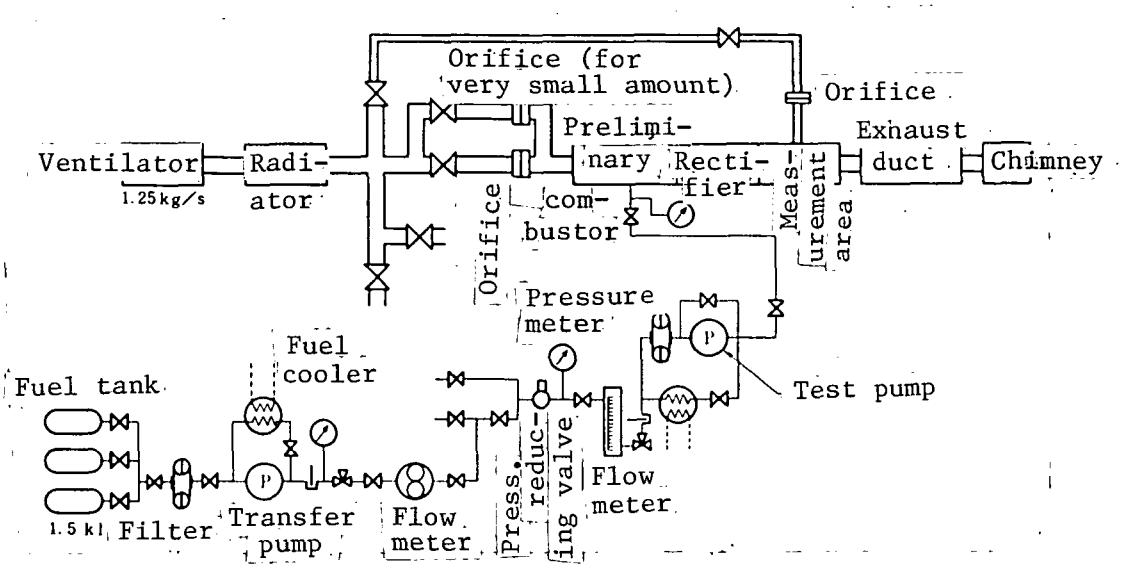

Figure 1. The schematic of the test facilities

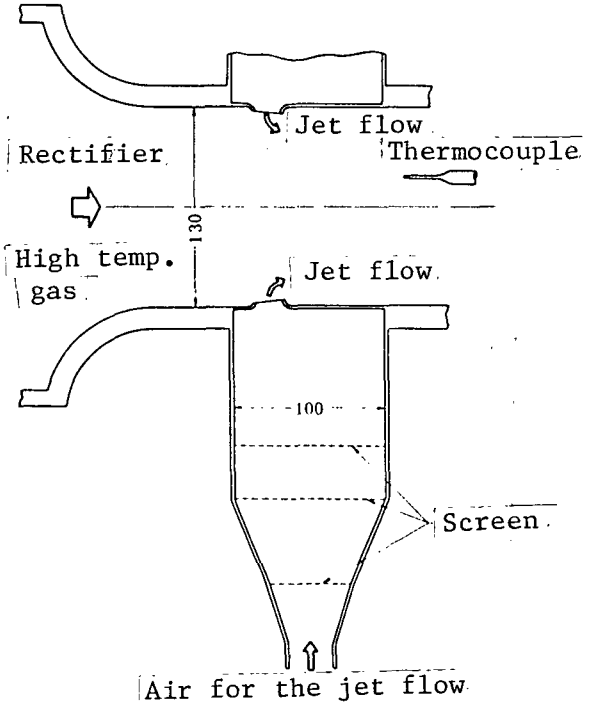

Figure 2. Test section of the round hole pairs

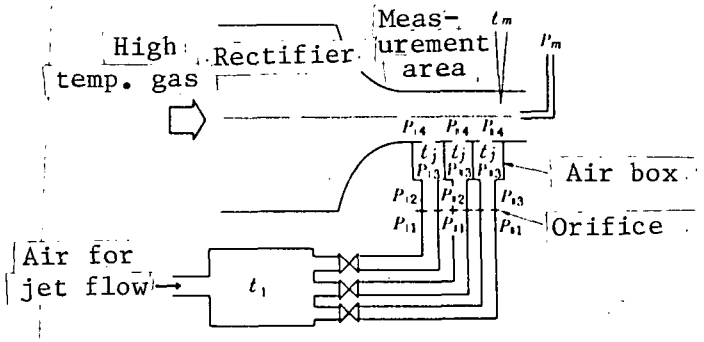

Figure 3. Measurement positions for the pressure and temperature

The three-holes were round air entry holes, as Figure 4 shows, installed along the three main flow directions on the bottom of the test section. The interval length ℓ between the air entry holes are either 20 or 50 mm, and numbers 9 and 10 are assigned to each model, continuing from the previous report.

Figure 5 shows a single elongated hole, and there is a guiding tube on the side of the exit hole. In the part of the

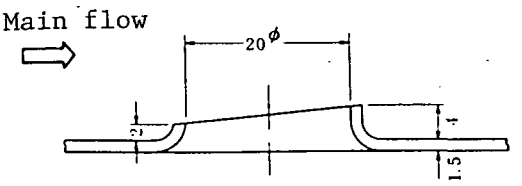

Figure 4. Shape of the air entry hole (Single round hole, No. 1; Straight line, three holes, Nos. 9, 10; Facing two-hole pairs, No. 14)

tube facing upstream in the main flow, a section of the guide tube was cut off following the example of the actual combustor. The original shape of the cut-off section of the guide tube was changed because the high temperature gas in the combustor burned it off. Experiments were made for three different heights of the guide tube: H = 5, 10, 15 mm and Nos. 11, 12 and 13 were assigned to these models.

The round-hole pairs were the round holes shown in Figure 4. They face each other on the top and the bottom of the test section, see Figure 2. The round air entry hole has the same shape as the single hole No. 1 shown in a previous report. The air entry holes facing each other are different from those on one side only. In the former case the jets from the air entry holes collide when the velocity of the flows is high. There was only one model of this kind, and No. 14 was assigned to it.

Figure 6 shows an example of the air-entry-holes model, and Figure 7 shows the test section of the round-holes pairs and the thermocouple displacement system.

For the experiment, the temperature measurement in the flow was done by changing the temperature and velocity of the main flow and the velocity of the jets. The temperature measurements were done using a 0.3 mm probe. The exposed Chromel-Alumel thermocouple and radiation compensation were omitted. For the measurement of the electromotive force, a PRO - 12 type X-Y Recorder by Yokokawa Electric Company was used. The temperature and the velocity of the main flow were obtained from the from thermocouples and total pressure tubes. The velocity of the jet flow was obtained on the basis of the compression difference between

the air entry hole side and exit hole side. The flow volume of the jet flow was obtained from a special orifice.

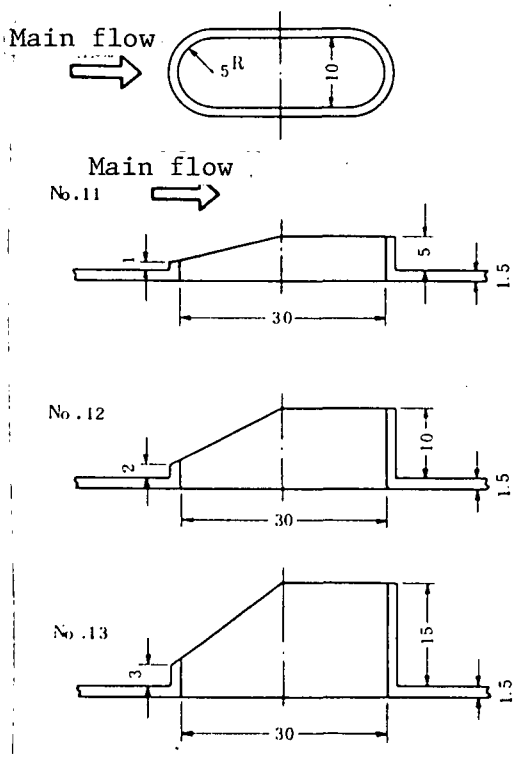

Figure 5. Elongated model

3. Results of the Experiment

The results of the experiment have been classified according to air entry holes flow coefficient, flow motion, jet flow intensity of penetration, shape of the isotherm and mixing of the jets. A formula was derived from the experiment with each air entry hole and it was compared with the results for single round hole No. 1. /3

3.1. Flow coefficient of air entry hole

The flow coefficient of each air entry hole model is obtained from the following formula based on the pressure difference of the back and front of the air entry hole (P_3 - P_4) and the "gravity flow" of the jet G measured at the orifice.

$$C_i = \frac{G_{j\,i}}{\varepsilon_i A_a \sqrt{2g\,(P_{3,i} - P_{4,i})\,\gamma_{3,i}}} \qquad (i = \mathrm{I},\ \mathrm{II},\ \mathrm{III}) \tag{1}$$

Here:

Aa: cross section area of the air entry hole

g: acceleration of gravity

γ_3: the specific gravity of the air at the entry point of the air entry hole

ε: the correction coefficient for the air expansion as it passes through the air entry hole

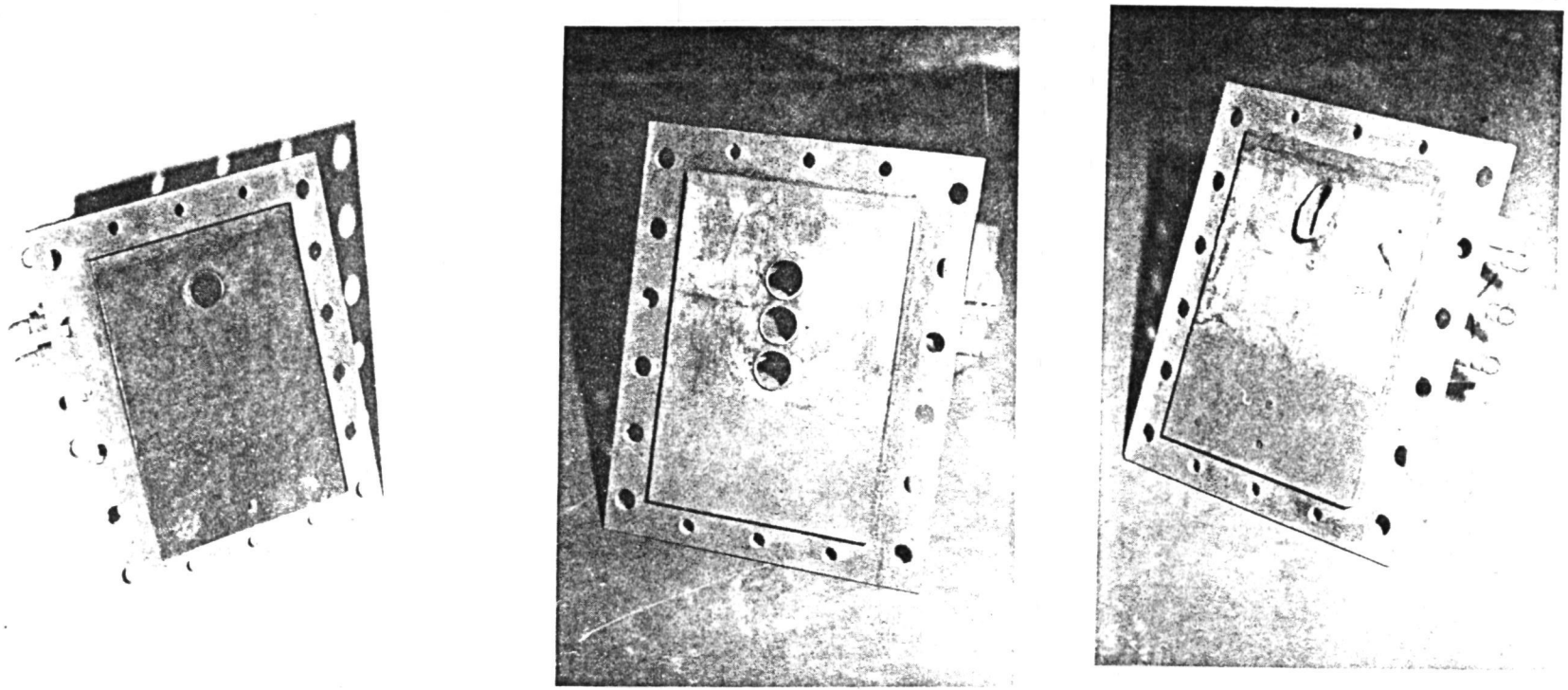

(a) Single round shaped hole No. 1

(b) Straight line three holes, No. 9

(c) Elongated hole No. 13

Figure 6. The air entry hole model

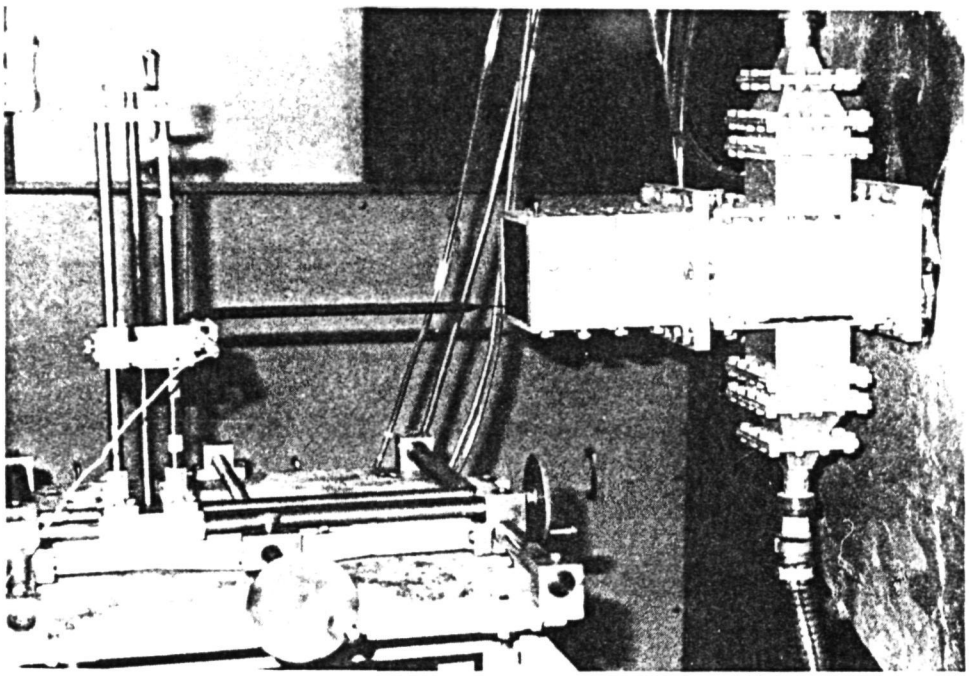

Figure 7. View of the test section (facing-hole pairs)

The measurement P_4 was done using "a static pressure probe" installed on the wall of the test section 15 mm away from the center of the air entry hole and perpendicular to the main flow.

The flow coefficient of the three holes is shown in Figure 8. The measurements were made for the same amount of flow through each hole. For a low momentum ratio, the flow coefficients of the three holes are lowest at hole No. I on the upstream side, close to 1.0 at hole No. II in the middle. The mean value for holes Nos. I and II equals the value for No. III on the downstream side. We can surmise that the hole No. I is under direct influence of the main flow, that there is almost no influence on hole No. II and a slight influence on hole No. III. The flow coefficient of hole No. I is lower than that of the single hole No. 1. Here the momentum ratio is low. We think we can account for this due to the increase in the main flow acceleration caused by the large total flow in thejet and the increased collision between the No. I jet and the main flow because there are jet flows from the holes Nos. II and III. In the case of three holes No. 10, the intervals between the air entry holes are longer, and the

/6

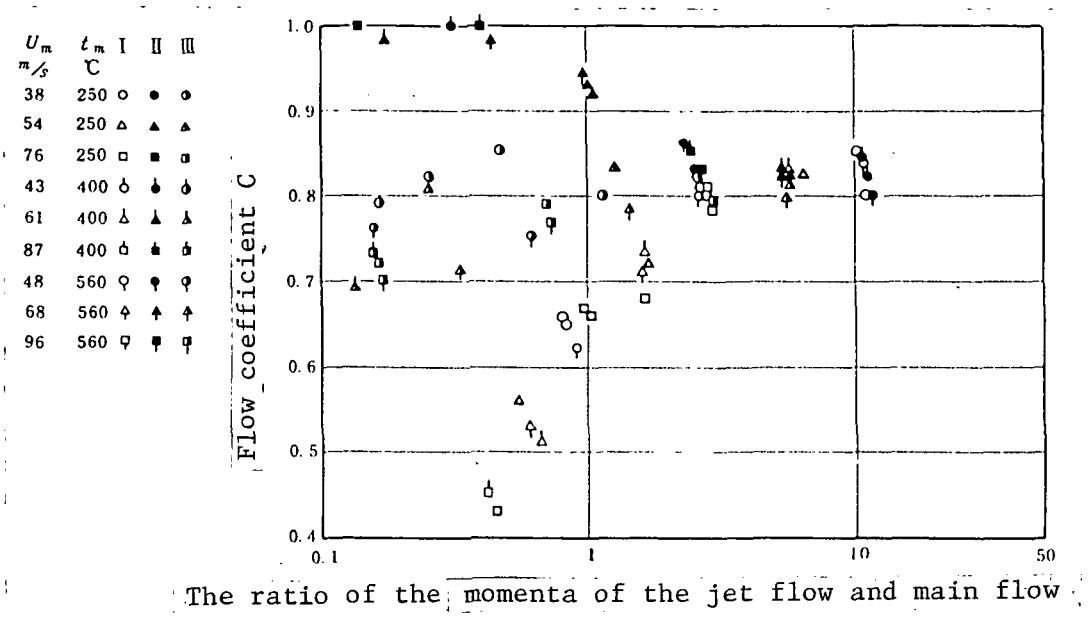

Figure 8. Flow coefficient of the three holes in a straight line, No. 9

value tends to approach the value of single air entry hole No. 1.

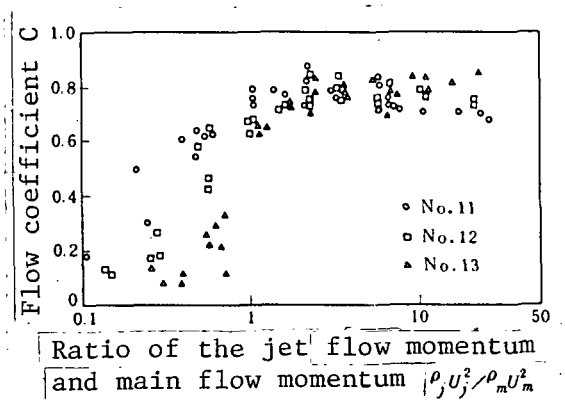

Figure 9. Flow coefficient of the elongated hole

Figure 9 shows the flow coefficients of elongated holes Nos. 11, 12, and 13. The change in the momentum ratio of the flow coefficient tends to indicate a similar effect as for single round hole No. 1. A comparative experiment based on the different heights of the guide tubes shows that, when the momentum ratio is small, the largest flow coefficient exists in No. 11 with a low guide tube. As the guide tubes become higher, the flow coefficients become smaller. This is because this is an area where the influence of the main flow is large and part of the main flow is accelerated by the guide tube. The degree of acceleration becomes larger when the guide tube height increases. We can assume that the higher the guide tube is, the more the dynamic pressure is captured in the front. The jet flows as it is being pressed down hard on the side of the downstream side of the guide tube. Where the momentum ratio is large, the flow coefficient

tends to be low if the height of the guide tube is small. We think this is because, when the influence of the main flow is weak and when the flow coefficient is determined by the flow of the jet flow itself, (it) is close to the flow through the orifice if the guide tube is low and it gets close to the flow near the entrance of the tube if the guide tube is large.

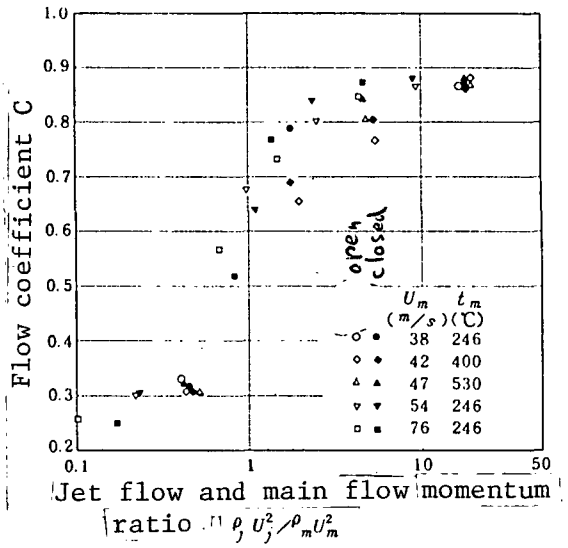

Figure 10.. Flow coefficient of the round two-hole pairs

The flow coefficient of the round two-hole pairs is shown in Figure 10. For the measurement, the same amount of air was allowed to flow through the air entry holes on the top and at the bottom, but the pressures at the rear and the front of the air entry hole were not exactly the same. This influence on the flow coefficient and the momentum ratio was noticed. There were no special trends in this difference between the top and bottom air entry holes. The change of the flow coefficient with the momentum ratio has shown the same tendency as in the case of the single round hole No. 1, but it showed a lower value than the single hole where the value of the momentum ratio is small. Our inference is that because of the limited cross section of the flow path in the test section, in spite of the fixed momentum ratio, the total flow of the jet from the two holes is larger than the single hole and the acceleration of the main flow increases.

3.2. The flow pattern of the jet flow

The flow pattern of the jet flow is shown by the isotherm shape obtained from the temperature distribution measured by the thermocouple. The penetrating power, the flow path and the mixture of the jet flows were also obtained on the basis of the isotherm, as was done in the previous report.

3.2.1. The flow pattern

The flow pattern of the jet flow was obtained from the isotherm which connects the points which are equivalent to the difference Δt between the temperature of the main flow t_m and the temperature of each part of thejet flow t_j, that is, $\Delta t = t_m - t_j$. Figures 11 - 13 show the flow pattern inside the cross section along the main flow. The flow pattern for the three holes No. 10 shown in Figure 11 is a complicated one. It shows the flow from each air entry hole along the upstream part. The shape is similar to the flow from the single round hole in which each individual jet is mixed downstream. The pattern of the flow from the elongated hole in Figure 12 is similar to the pattern of the flow for the single round hole. The same figure shows that the velocity of the jet flow increases with an increase in penetrating power of the jet flow. The flow pattern of the facing round tow hole pairs in Figure 13 shows that the two jet flows interfere as the velocity of the jet flow increases. The flow [illegible] becomes different from the flow of the single round hole. Downstream in Figure 13 (d), which shows the highest velocity of jet flow, the lowest temperature over the cross section shown by the dotted line occurs in the center of the flow path.

The flow pattern in the cross section perpendicular to the main flow is shown in Figures 14 and 15. The shape of the isotherm in Figure 14 is almost the same with the same effect of the round air entry hole [2] when the jet flow velocity is low. Where the jet flow velocity is high, the isotherm in the lateral direction was narrower than in the case of the round air entry hole. For the round entry hole, a cross section up to $\bar{x}$ = 140 mm, it was observed that two places in the lowest temperature part were formed as a pair. In the elongated hole there was only one place in the /10
part of each cross section where the central axis of the jet flow is formed. We tend to think that the jet flow is pressed by the side of the guide tube on the backflow side where the jet flow velocity is low. Because of this there was no big difference in the shape of the jet flow cross section between the two air

entry holes.

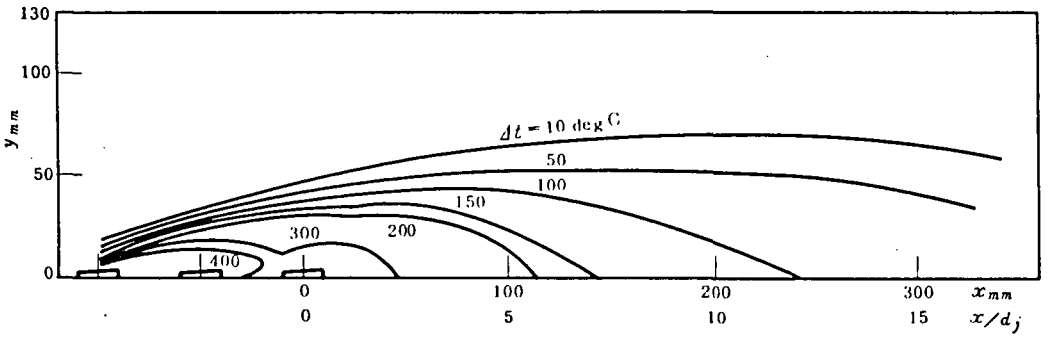

a) $U_{j\,\mathrm{I}} = 30.6\,\mathrm{m/s}$ $U_{j\,\mathrm{II}} = 20.4\,\mathrm{m/s}$ $U_{j\,\mathrm{III}} = 24.2\,\mathrm{m/s}$ $t_{j\,o} = 27\,^{\circ}\mathrm{C}$

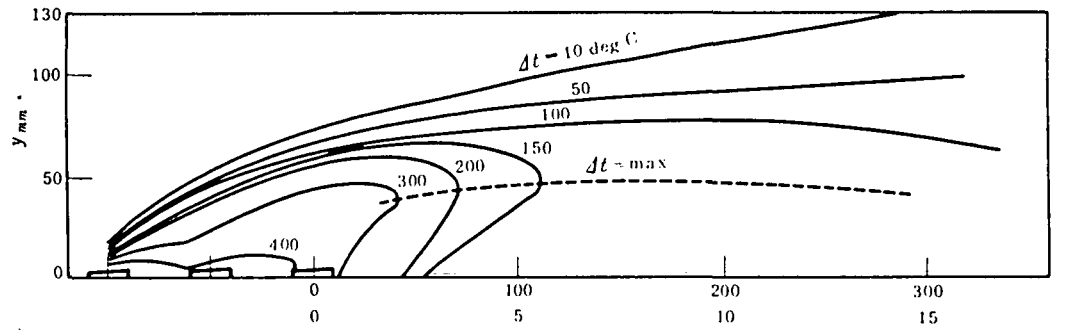

b) $U_{j\,\mathrm{I}} = 50.5\,\mathrm{m/s}$ $U_{j\,\mathrm{II}} = 44.4\,\mathrm{m/s}$ $U_{j\,\mathrm{III}} = 48.0\,\mathrm{m/s}$ $t_{j\,o} = 29\,^{\circ}\mathrm{C}$

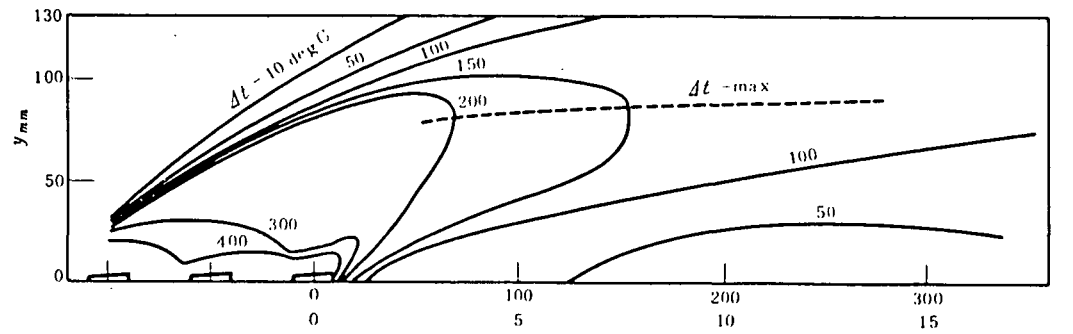

c) $U_{j\,\mathrm{I}} = 93.9\,\mathrm{m/s}$ $U_{j\,\mathrm{II}} = 90.9\,\mathrm{m/s}$ $U_{j\,\mathrm{III}} = 95.1\,\mathrm{m/s}$ $t_{j\,o} = 29\,^{\circ}\mathrm{C}$

Figure 11. Temperature distribution of three holes No. 10
$U_m = 67.9\,\mathrm{m/s}$ $t_m = 556\,^{\circ}\mathrm{C}$

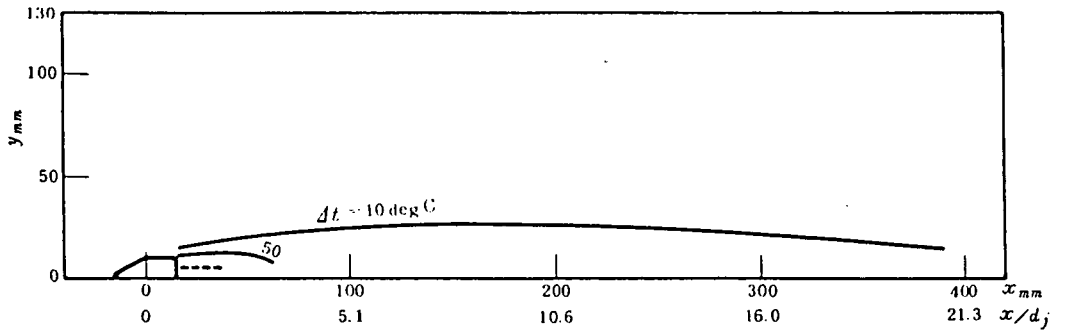

a) U_j = 22.4 (m/s) t_j = 30(℃)

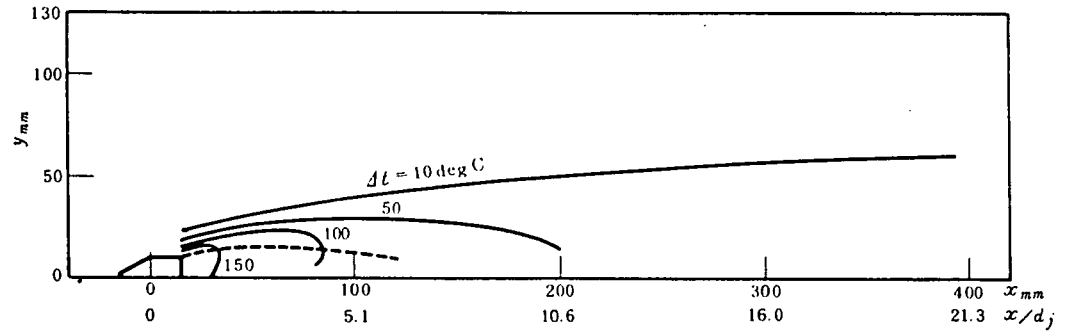

b) U_j = 41.3 (m/s) t_j = 32(℃)

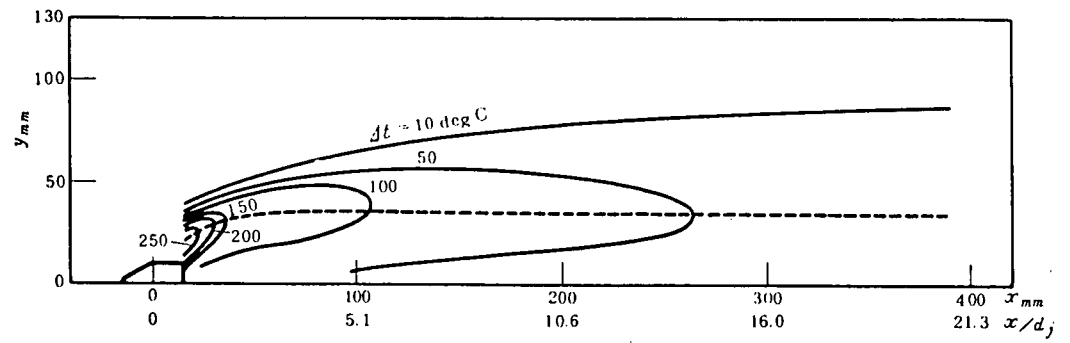

c) U_j = 74.9 (m/s) t_j = 32(℃)

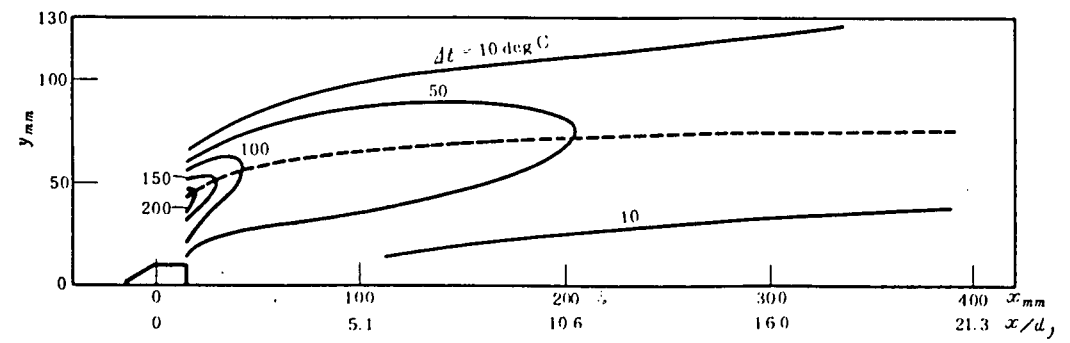

d) U_j = 135.8 (m/s) t_j = 33(℃)

Figure 12. Temperature distribution of the elongated hole No. 12

U_m = 60.3 (m/s) t_m = 390.3(℃)

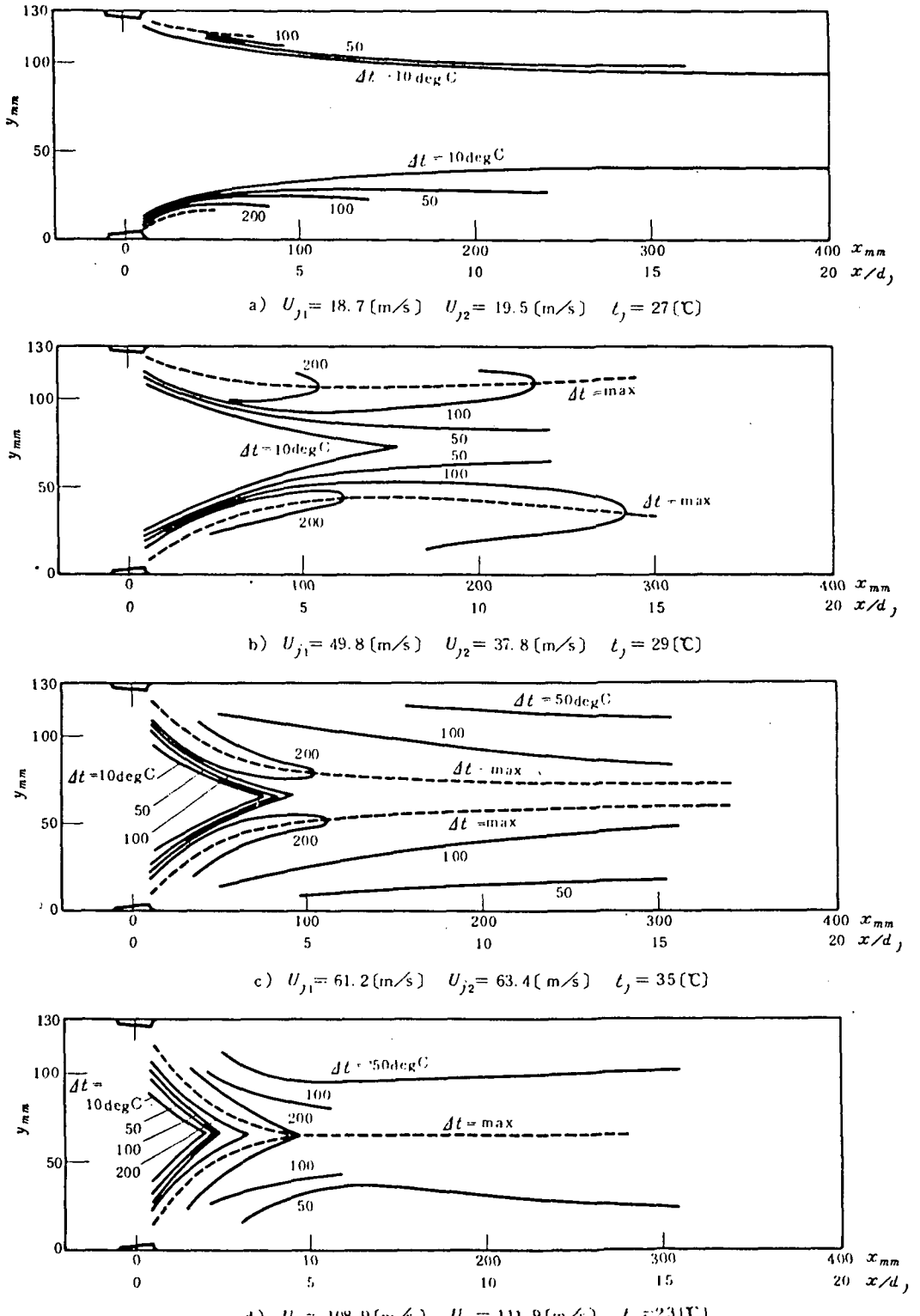

Figure 13. Temperature distribution for round, two-hole pairs
U_m= 47.2 (m/s) t_m= 532 (℃)

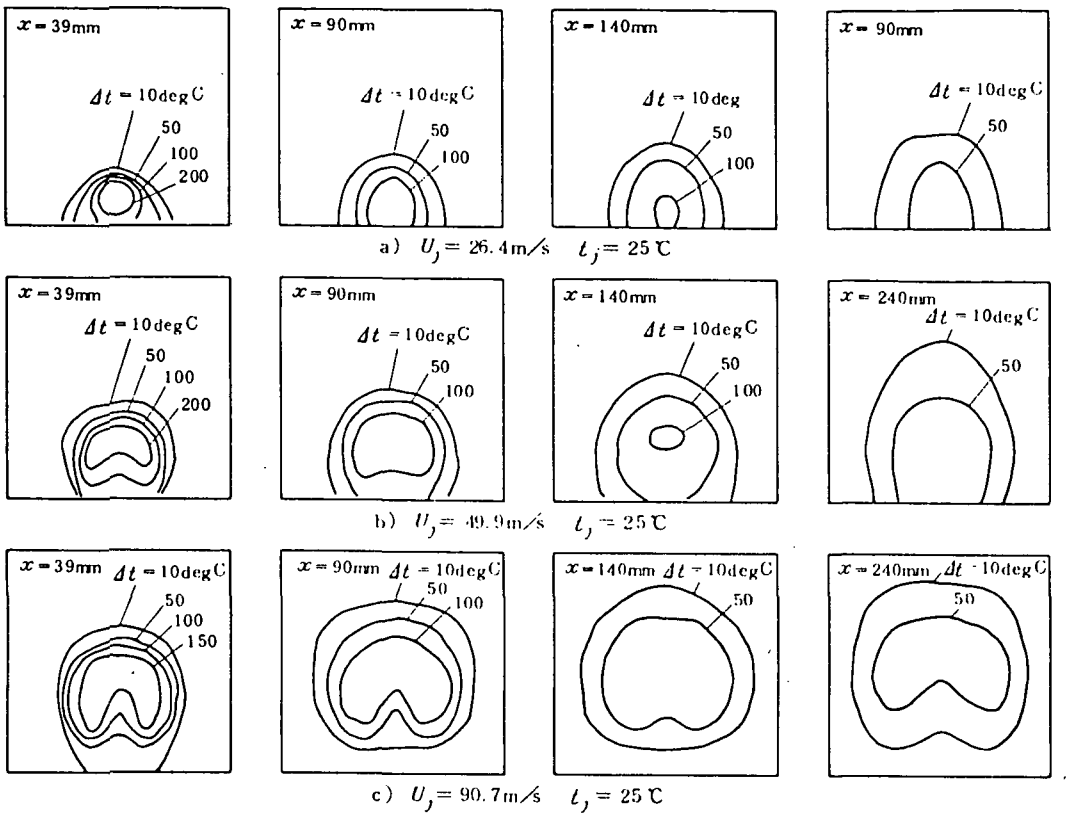

Figure 14. Temperature distribution of the elongated hole No. 12 U_m= 48m/s t_m=550℃.

The measurement results for the pair of facing round holes shown in Figure 15 shows that, where the jet flow velocity is low, each jet flow has a similar cross sectional pattern to that of the jet flow from a single round hole. Where the velocity was high, the two jet flows mixed. Figure 15-2(c) shows a formation of low temperature area due to jet mixing in the central section of the flow path. Figure 15-2(d) shows that where the jet flow velocity was high, the jets flow on top and bottom with a horse-shoe shaped cross section and become mixed. They formed a pair of low temperature areas on the left and right sides. Under different conditions, we could observe that, during the formation of the pair of low temperature areas to the left and right, the pair of low temperature areas in each jet flow developed. As a consequence, there were cases where a total of four low temperature areas were recognizable. When the velocity of the jet flow decreased further, the temperature tended to level off even on the

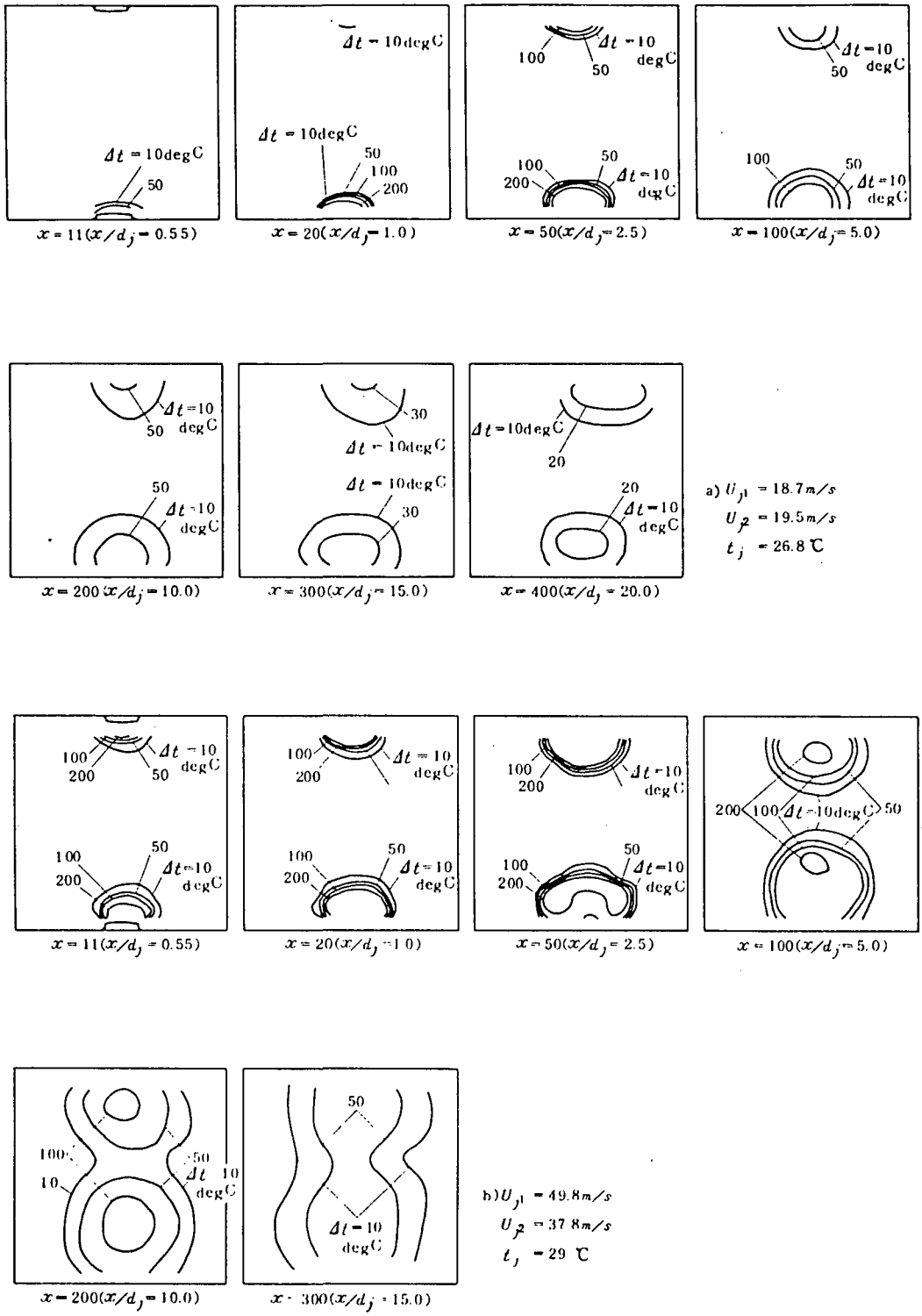

Figure 15-1. Temperature distribution of the pair of facing round holes U_m= 47.2m/s t_m= 532℃

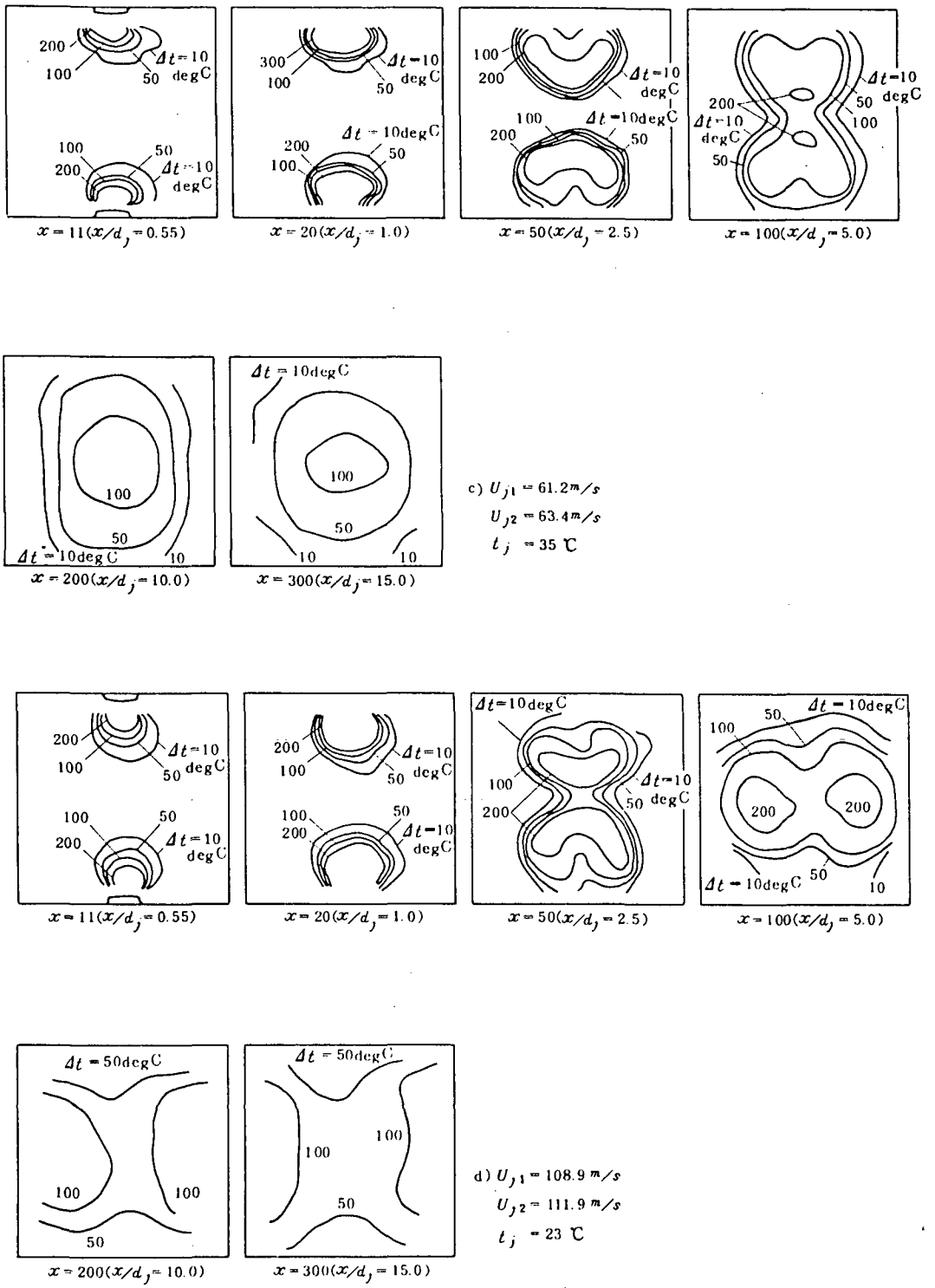

Figure 15-2. Temperature distribution of the pair of facing round holes U_m= 47.2m/s t_m= 532℃.

left and the right, and the temperatures at the center of the flow path on the top and the bottom were low. The temperature near the wall face of the downstream jet flow hole was high. This occurs, we think, because as the jet flows collide almost head-on, they spread in the lateral direction and near the wall face where the jet flow holes are, the main flow circulates around the jet flows.

3.2.2. Intensity of penetrating power

The measure for the penetrating power used here was the ratio Y/d_j, in which Y represents the isotherm in which the temperature Δt was fixed, or Y corresponds to the maximum range in the direction y along the line which connects the lowest temperature points of the jet flow. d_j represents the diameter of the air entry hole or major axis of the elongated hole. It was also expressed as $(Y - H)/d_j$ where H is the height of the guide tube.

Figure 16 shows the result of the adjustment on the penetrating power of the jet flow for the three holes. The value of Y was taken from the face of the wall and it was adjusted according to the formula (2) using a shape similar to the single round hole shape. The values of ℓ, m, β are shown in Table 1.

$$\frac{Y}{d_j} = \ell \left(\frac{\Sigma \rho_j U_j}{\rho_m U_m} - m \right)^{\beta} \qquad (2)$$

Here, ρ: density, U: velocity ℓ, m, β: affixes to the constants, j: jet flow, and m: main flow.

Figure 17 shows a comparison of the result of the three holes No. 9 and a single round hole. In the figure, the estimated values were obtained by substituting the values obtainable from the three holes as a value of the mass ratio in the formula for the single round hole. The estimated values and the actual measured values on the basis of this method coincided for the two holes in a straight line [2]. In Figure 17, the actual measured values were lower than the estimated values. In the case of two holes, /13

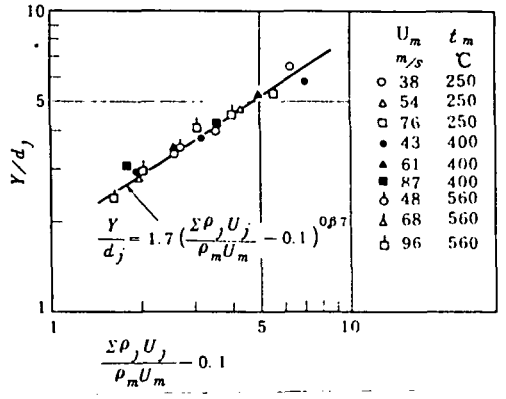

Figure 16. The penetrating power of the three holes No. 9 ($\Delta t = 10$degC).

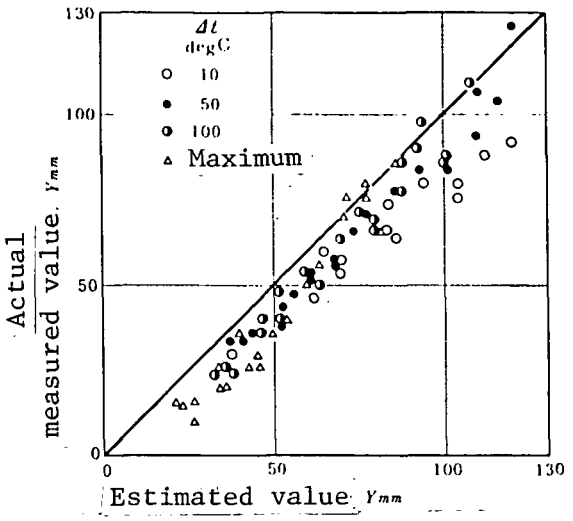

Figure 17. Correlations between the estimated values and the actual measured values of the maximum penetration distance of three holes No. 9

TABLE 1. THE VALUES OF ℓ, m, β

Type of air entry hole	No.	Air intake hole interval L,mm	Δt degC	ℓ	m	β
3 holes in a straight line	9	25	10	1.7	0.1	0.67
			50	1.2	0.25	0.72
			100	1.0	0.5	0.73
			max	0.6	0.8	1.0
	10	50	10	1.7	0.1	0.67
			50	0.8	0.25	1.0
			100	0.7	0.5	0.93
			max	0.5	0.8	0.8
Elongated hole	11 12 13	—	10	2.7	0.5	0.48
			max	1.0	1.0	0.93

the jet flow from the two holes mixed and showed a flow similar to the flow with a volume equivalent to two holes and flowing from a single air entry hole. We could assume the extent of mixing was small because the distance between the air entry holes was large. The result of the model No. 10, with long intervals between the air entry holes also showed a tendency as Figure 17 shows. Because the effect of the mixing was small when the value of Y was small, there was a strong tendency for the actual measured values to become smaller than the estimated values.

The effect of Δt = 10 degC measured in the elongated hole model is shown in Figure 18 and the effect of Δt = max is shown in Figure 19. The value of d_j for the elongated hole is the value of the diameter of a circle with the same area as the open hole area of the elongated hole. This could be compared with the

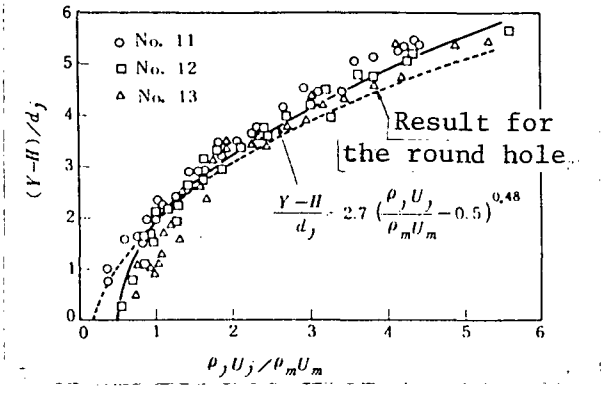

Figure 18. Penetrating power of the elongated hole ($\Delta t = 10$ deg C).

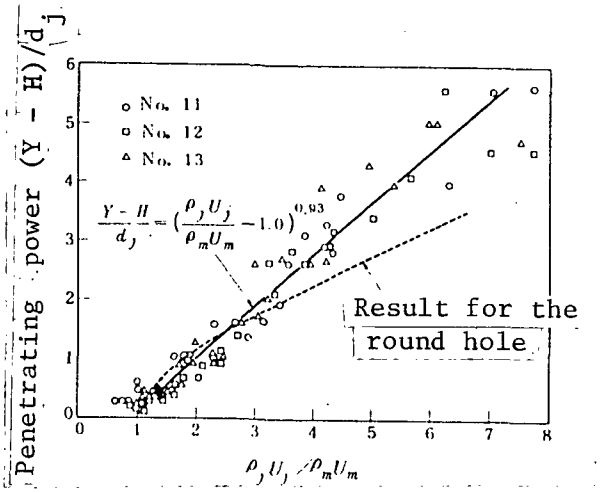

Figure 19. Penetrating power of the elongated hole ($\Delta t = \max$).

effect of the round air entry hole. The elongated hole used for the experiment had d_j = 18.8 mm. For the adjustment, with consideration of the height H of the guide tube, the following formula was used which is similar to formula (2). /14

$$\frac{Y-H}{d_j} = \ell\left[\left(\frac{\rho_j U_j}{\rho_m U_m}\right) - m\right]^{\beta} \qquad (3)$$

The adjusted result shows that, for Δt = 10 deg C, a slightly greater penetration power occurred in No. 11 for which the height of the guide tube is low. For Δt = max, there was a considerable dispersion but the results of the elongated hole models No. 11, 12, and 13 agreed with the constants ℓ, m and β of formula (3). The values of ℓ, m, and β are shown in the figure and in Table 1. The results prove that the height of the guide tube has a direct effect on the increase and decrease of the penetration power. We assume such a simple adjustment becomes impossible because there is also an influence from the height of the flow path when the height of the guide tube becomes as high as the height of the flow path in the test section. Compared to the round air entry holes, when the value of the mass ratio $\rho_j U_j / \rho_m U_m$ is large, the penetration power of the elongated hole is greater as Figures 18 and 19 show.

In Figure 20, the penetration of the jet flow from the

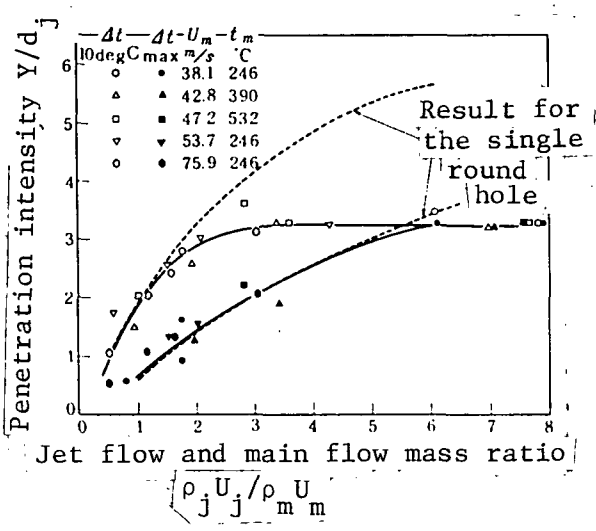

Figure 20. The penetration intensity of the jet flow from the bottom side air entry hole of the pair of facing holes

two-hole pairs and results for the single round hole are shown. Figure 20 shows that two jet flows collide where the mass ratio $\rho_j U_j / \rho_m U_m$ of the jet flow and the main flow is large and the value of the penetration intensity is near $Y/d_j = 3.25$ which is the center of the flow path. The figure corresponds to the bottom side air entry hole. Similar results were found for the air entry hole on the top. In comparison to the result for the single round hole, the penetration intensities were about the same when the mass ratio was Δt = 10 deg C and Δt = max was small. On the other hand, when the value of the ratio is large, the penetration of the pair of facing holes became small because of the collision. The collision effect was great for the isotherm Δt = 10 deg C which shows the outer circumference of the jet flow and there was a difference due to the smaller value of the mass ratio for Δt = max.

3.2.3. Path of the jet flow

We investigated the change in the isotherm which passes through the center of the air entry hole along the main flow in the cross-section and the change in the line which connects the points of Δt = max equivalent to the center of the jet flow.

Figure 21 shows the result from the isotherm Δt = 10degC of the jet flow from the three holes. The limits of the data shown in the figure are between $x/d_j = 1.5 \sim 15$ where the center of the hole No. III is the original point of x and at the same time in the section before the isotherm became parallel to the main flow. The solid line in the figure is the calculated value by substituting the mass ratio of the (air) volume for three holes in the

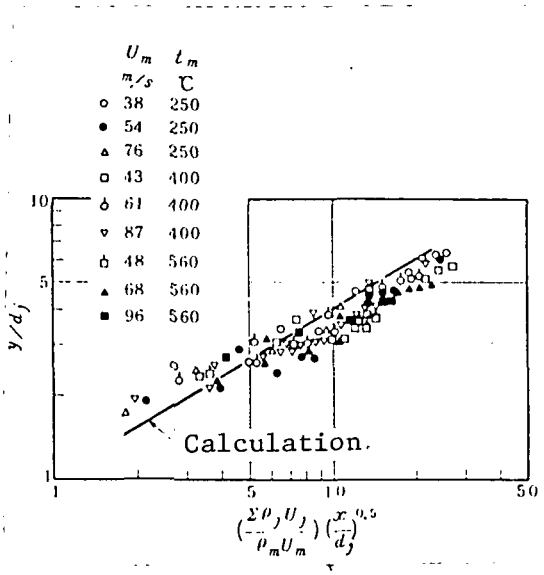

Figure 21. The path of the jet flow (three holes No. 9)

test formula for the single round hole and by taking the center of the hole No. III for the original point of x. Considering that the result for two holes agreed well with the similar computed value, the measurement result for three holes showed that the penetration intensity of the jet flow was large where the abscissa value in Figure 21 was small. It became small where the value of the abscissa value was large. The cause for this difference was found by investigating the data adjustment of each measurement location along the x direction. It was caused by the tendency shown in Figure 22. This tendency appeared when the temperature difference Δt was large. This also occurred for model No. 10, whose air entry hole intervals are much longer. The reason why the measured value from the three holes on the downstream side is lower than the computed value is because the mixing of the jets was low and because the computed penetration flow was low.

For the path of the jet flow from the elongated hole, we picked the isotherm Δt = 10degC and the line which connects the points of Δt = max which corresponds to the center of the jet flow. The measurement values are between x/d_j = 4 ∿ 10 and 1.4 ∿ 10 for the former and the latter, before the two lines became parallel to the main

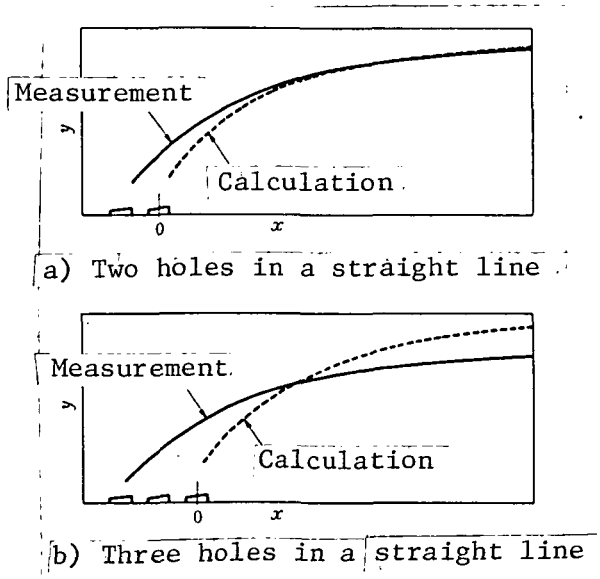

Figure 22. Path of the jet flow

flow. For the isotherm of Δt = 10 degC, based on the result of the round hole which was adjusted by using the mass ratio, it was adjusted as in Figure 23 in the form

$$\left(\frac{y-H}{d_j}\right)^{1.32} = 0.7\frac{\rho_j U_j}{\rho_m U_m}\left(\frac{x}{d_j}\right)^{1/2} \tag{4}$$

For the line connecting the points of Δt = max, the adjustment based on the mass ratio showed a large dispersion and the following formula which uses the momentum ratio instead of the mass ratio of formula (4), which had a coherent form as shown in Figure 24. /15

$$\left(\frac{y-H}{d_j}\right)^{1.7} = 0.24\frac{\rho_j U_j^2}{\rho_m U_m^2}\left(\frac{x}{d_j}\right)^{1/2} \tag{5}$$

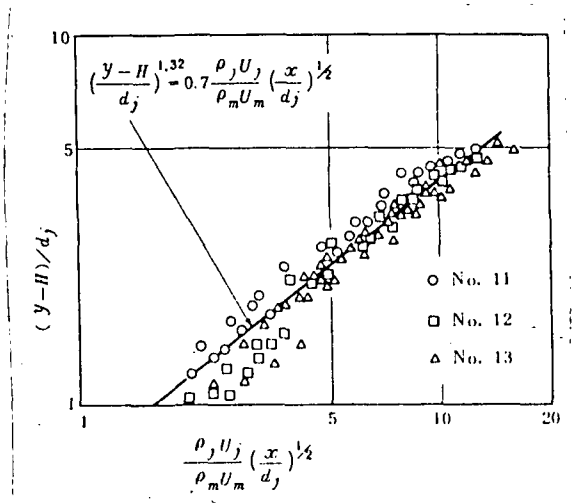

Figure 23. Path of the jet flow (elongated hole, Δt=10 degC)

$1 \leqslant \frac{\rho_j U_j}{\rho_m U_m} \leqslant 5.7,\ 4 \leqslant \frac{x}{d_j} \leqslant 10$

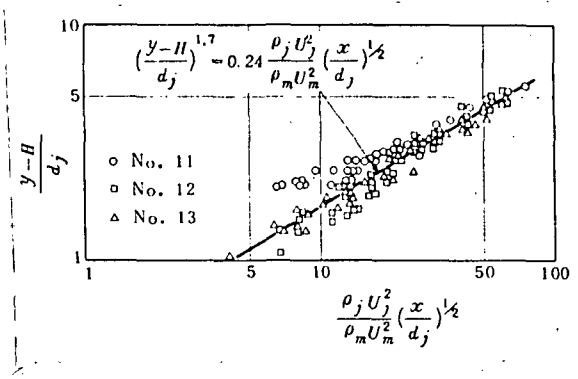

Figure 24. Path of the jet flow (elongated hole, Δt=max)

$3.3 \leqslant \frac{\rho_j U_j^2}{\rho_m U_m^2} \leqslant 26,\ 1.4 \leqslant \frac{x}{d_j} \leqslant 10$

Whether the mass ratio or the momentum ratio should be selected as the method of the data adjustment is probably determined by establishing which element is the controlling factor. We think that the penetration intensity and the path of the jet flow are controlled by the momentum ratio of both the jet flow and the main flow. For the isotherm of Δt = 10degC, the reason why there was a more coherent form when the data adjustment was done using the mass ratio could be due to the influence of the

height of the flow path and the change in the shape of the cross section. The shape of the cross section at the rear of the air entry hole is exactly the same as the shape of the air entry hole, and as the main flow gradually forms eddies, it looked like a shape crushed by the main flow. This cross-sectional change resulted in an increase in the resistance coefficient of the jet flow toward the main flow. And the jet flow became easy to bend. As a result, the penetration intensity of the jet flow decreased more than given by the shape of the cross section obtainable from the momentum ratio. A further decrease in the penetration intensity was expected around the outer circumference of the jet flow. A data adjustment in a coherent form using the mass ratio for the isotherm of Δt = 10degC could have been made. Because it is easier to maintain the penetration around the central section of the jet flow than around the outer circumferential section, we think an adjustment is possible using the momentum ratio between $1.4 < x/d_j < 10$ along the line Δt = max.

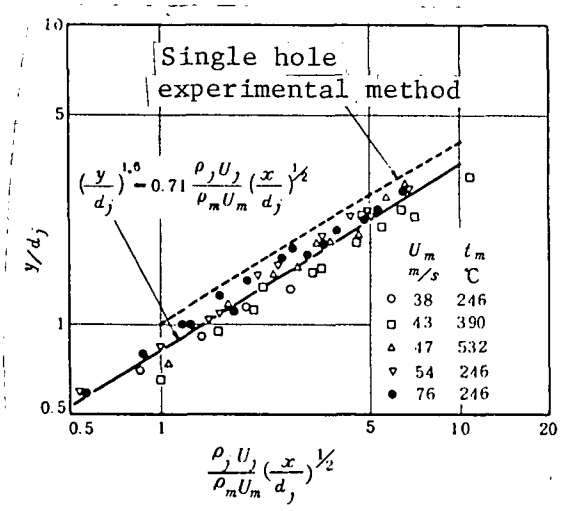

Figure 25. Route of jet stream (two opposing round holes, lower air hole, Δt=10degC)

$0.5 < \frac{\rho_j U_j}{\rho_m U_m} < 4.5, \quad 1.0 \leqq \frac{x}{d_j} \leqq 10$

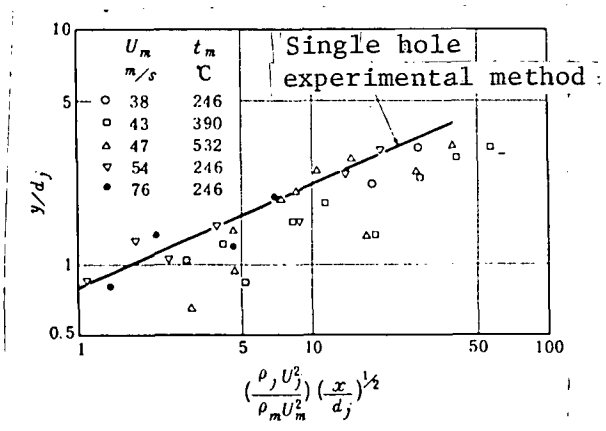

Figure 26. Route of jet stream (two opposing round holes, lower air hole, Δt=max)

$1.0 < \frac{\rho_j U_j^2}{\rho_m U_m^2} < 19, \quad 1.0 \leqq \frac{x}{d_j} \leqq 10$

Figures 25 and 26 show the adjustment of the data for the jet flow from the bottom side air entry hole of the pair of round holes. Figure 25 corresponds to the isotherm Δt = 10degC and there is a considerable dispersion of the data. It can be represented by the formula

$$\left(\frac{y}{d_j}\right)^n = 0.71\frac{\rho_j U_j}{\rho_m U_m}\left(\frac{x}{d_j}\right)^{1/2} \qquad (6)$$

Comparison of this result with the value of the single hole shown by the dotted line in the Figure shows that the penetration of the two hole jet flow has become low. The result from Δt = max of Figure 26 shows a large dispersion. About half of the total data indicates the same penetration intensity as for the single hole. Because of the decrease in the penetration intensity of two-hole jet flow was very clearly noticeable when the velocity of the jet flow was highest; the mutual interference of the jet flows around the outer circumference of the jet flow for Δt = 10 deg C became low in other cases.

3.2.4. Degree of mixture /16

The extent of uniform temperature which develops when the jet stream mixes with the primary stream is given by the degree of mixture R_t defined in equation (7) below. The changes in the extent are studied.

$$R_t = \frac{t_{min} - t_j}{t_o - t_j} \qquad (7)$$

Wherein t_{min}: minimum temperature at each cross section of air hole downstream, t_1: temperature of jet stream in air chamber, t_o: temperature upon complete mixture of primary stream and jet stream.

Figure 27 illustrates the degrees of mixture based on the mass flux ratio. It discloses that the minimum value is in the region where the velocities of the primary stream and of the jet stream are equal. In addition, rapid mixture takes place near the air hole, as shown in figure 28, since the angle and

temperature difference between the primary stream and the jet stream are great. On the downstream side, mixture occurs at a slower rate since the angle and temperature difference is smaller. These trends are similar to the results in the case of a single round hole.

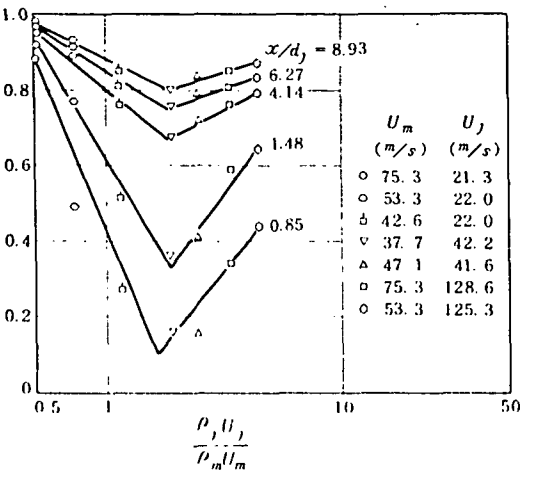

Figure 27. Degree of mixture - mass flux ratio (T_j/T_m : 0.52 No. 12 H = 10 mm

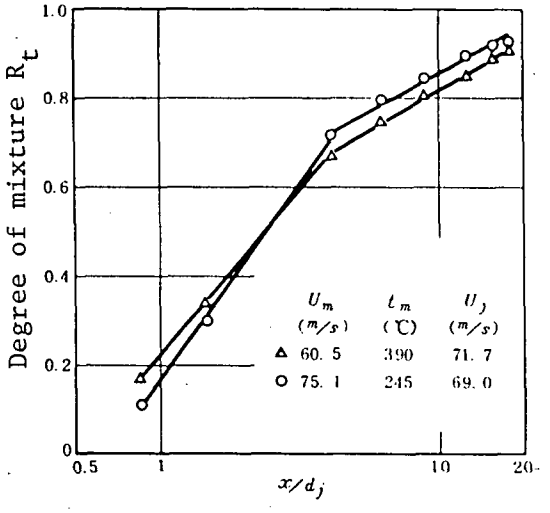

Figure 28. Change in degree of mixture in flow path direction. No. 13 H = 15 mm

Figures 29, 30 and 31 illustrate changes in the degree of mixture based on the mass flux ratio $\rho_j U_j/\rho_m U_m$ and on the distance x/d_j. Based on these results, the following experimental equation was derived.

$$R_t = \log\left\{\left(\frac{\Sigma \rho_j U_j}{\rho_m U_m}\right)^a \left(\frac{x}{d_j}\right)^q\right\} + b \qquad (8)$$

Table 2 illustrates the constants a, q, b of equation (8) and their applicable ranges. The form of the experimental equation is similar to that determined by conducting simple dimensional analysis on the single round hole.

Figure 32 compares the changes in the direction of flow of the degree of mixture of each air hole based on the resulting empirical equation. The mass flux ratio used in the comparisons was $\rho_j U_j/\rho_m U_m = 3$. Since the applicable range of the empirical equation of a series of three holes is greater than this value, the comparisons were made under the conditions of $\rho_j U_j/\rho_m U_m = 9$

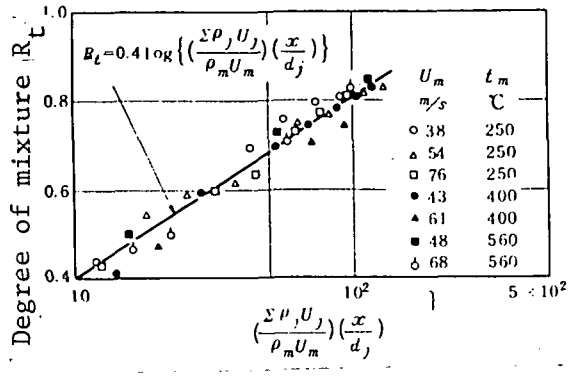

Figure 29. Degree of mixture (series of three holes (No. 10)

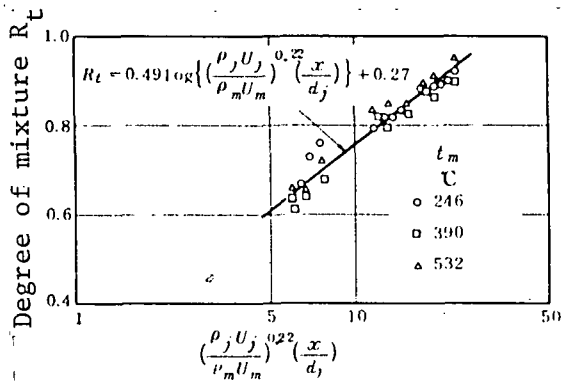

Figure 31. Degree of mixture (two opposing round holes)

$2<\frac{\rho_jU_j}{\rho_mU_m}<8,\quad 5<\frac{x}{d_j}<20$

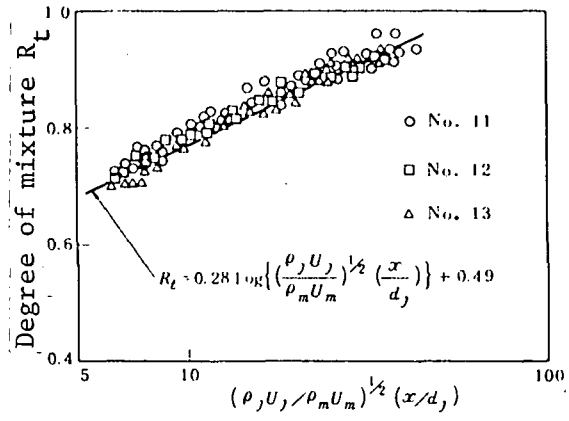

Figure 30. Degree of mixture of long hole $2<\frac{\rho_jU_j}{\rho_mU_m}<5.2,\quad 4<\frac{x}{d_j}<21$

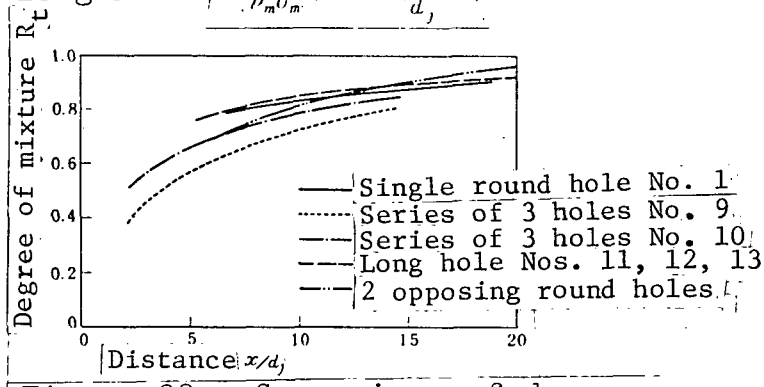

Figure 32. Comparison of degrees of mixture

TABLE 2. VALUES OF a, q, b

Designation	Model number	a	q	b	Range of application
Single round hole	1	0.25	0.48	0.35	$2<\frac{\rho_jU_j}{\rho_mU_m}<6,\quad 6<\frac{x}{d_j}<20$
Series of 3 holes	9	−0.50	0.50	0.7	$6<\frac{\Sigma\rho_jU_j}{\rho_mU_m}<10,\quad 2<\frac{x}{d_j}<15$
	10	0.40	0.40	0	
Long hole	11 12 13	0.14	0.28	0.49	$2<\frac{\rho_jU_j}{\rho_mU_m}<5.2,\quad 4<\frac{x}{d_j}<21$
2 opposing round holes	14	0.11	0.49	0.27	$2<\frac{\rho_jU_j}{\rho_mU_m}<8,\quad 5<\frac{x}{d_j}<20$

at which the mean flux ratio per each of the three air holes would be equal. The figure discloses that the degrees of mixture of the single holes overall were very close. The values of the series of three holes with different comparison conditions were lowest. The changes in the degree of mixture based on the mass flux ratio were striking when the value of a in equation (8) was high. In the experiment, the single round hole and the series of three holes correspond.

3.2.5. Temperature distribution shape within jet stream

Figure 33 illustrates the temperature distribution pattern within the jet stream which was determined identically to the method discussed in the previous report. Figures 34 and 35 illustrate the temperature distribution patterns respectively for No. 9 series of three holes and for No. 13 long hole. Both figures illustrate similar distribution patterns. The region of low temperature in the center of the jet stream is broader than in the distribution pattern of the cold free jet stream [3]. Abrupt temperature change in the peripheral section is evident. This tendency is also exhibited in the single round hole and in the series of two holes in the previous report. The data in Figures 34 and 35 illustrate the distribution on the upper side from the center of the jet stream discharging from the lower wall of the measurement section. The upper side is a position at which the peripheral section of the jet stream is directly affected by the primary stream. This is related to changes in the jet stream profile shown in the flow model.

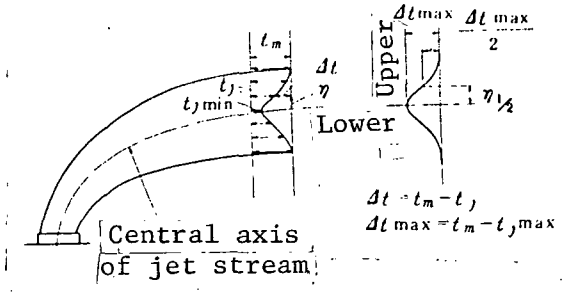

Figure 33. Method of determining pattern of temperature distribution

/19

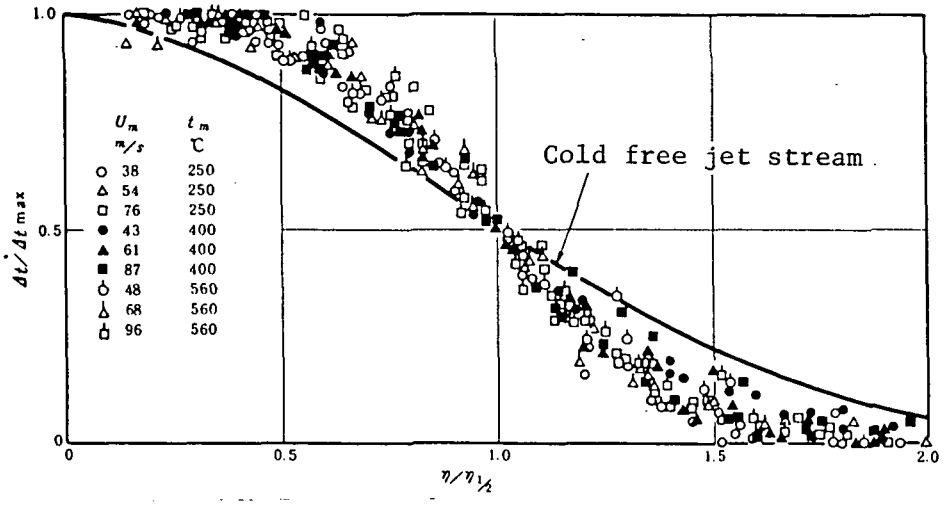

Figure 34. Pattern of upper temperature distribution of central axis of jet stream (series of 3 holes No. 9, $4 < x/d_j < 15$)

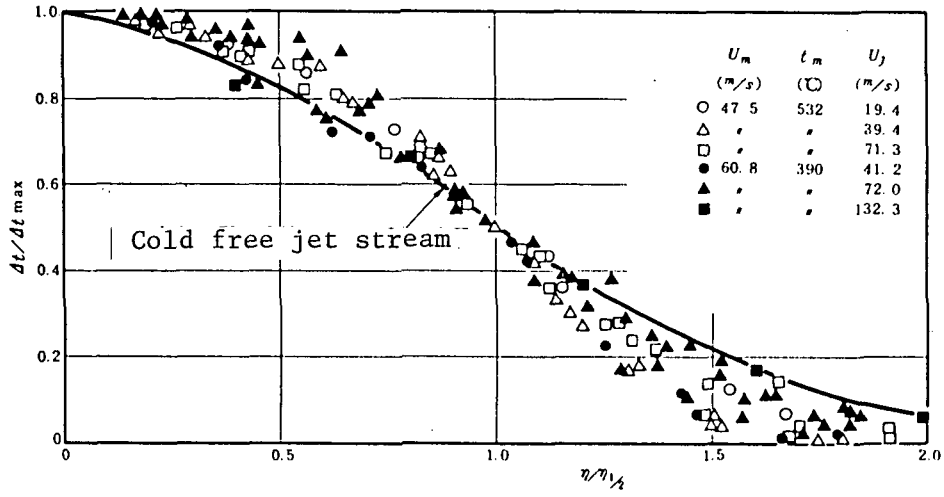

Figure 35. Pattern of upper temperature distribution of center of jet stream (long hole NO. 13, $4 < x/d_j < 21$)

4. Supplement of Single Round Hole Results

Since the results of Δt = max were not illustrated in the path of the jet stream from the single round hole disclosed in the previous report, consolidation was conducted followed by illustration of the results. In addition, the comparison with the results collected in other research is also illustrated.

Figures 36 and 37 illustrate consolidations of data from

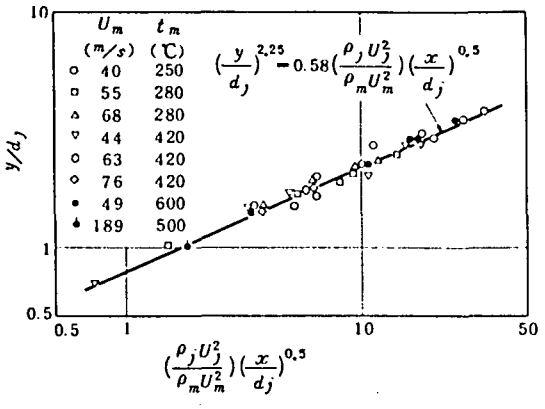

Figure 36. Jet stream path (single round hole No. 1 Δt = max)

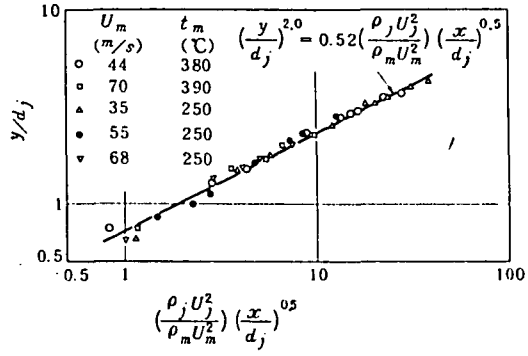

Figure 37. Jet stream path (single round hole No. 2 Δt = max)

single round holes Nos. 1 and 2 respectively. Air hole No. 1 has the form shown in Figure 4. The inlet is round with a diameter of 20 mm. Air hole No. 2 is not round, and has a diameter of 20 mm. Consolidation of the line linking Δt = max was achieved using the momentum ratio shown in Figures 36 and 37. The resulting experiments were

No. 1

$$(\frac{y}{d_j})^{2.25}=0.58(\frac{\rho_j U_j^2}{\rho_m U_m^2})(\frac{x}{d_j})^{1/2} \quad 0.24<\frac{\rho_j U_j}{\rho_m U_m}<6 \tag{9}$$

No. 2

$$(\frac{y}{d_j})^{2.0}=0.52(\frac{\rho_j U_j^2}{\rho_m U_m^2})(\frac{x}{d_j})^{1/2} \quad 0.6<\frac{\rho_j U_j}{\rho_m U_m}<6 \tag{10}$$

The range of x/d_j was 0.7 to 8.5. The line linking Δt = max on the profile through which passes the center of the air hole was parallel to the primary stream, as before. The minimum temperature of the jet stream is paired within the perpendicular profile to the jet stream, and there are also cases of its absence in the profile through which passes the center of the air hole. However, the method discussed above was adopted because of the complexity of the flow field. The data could be consolidated in a coherent form based on the momentum ratio rather than on the mass flux ratio because the inertia of the jet stream was maintained in the center, as in the study of long holes, and deformation of the jet stream profile had no direct effect.

Measurement of the path of the directly intersecting jet stream from the single round hole has been accomplished by various methods. Figure 38 compares the results achieved in this experiment with those from various other experiments. In the comparisons shown in the figure, the abscissa is in the form of $(\rho_j U_j/\rho_m U_m)\ (x/d_j)^{1/2}$. Results which could be consolidated in various ways have been reconsolidated based on the conditions shown in the figure. The results achieved in this experiment illustrate lower penetration over a broader range than in the case of other measurements. The reason is that the flow path height of the measurement section in this experiment, h/d_j, as shown in Table 3, is much lower than in other experimental devices, resulting in a flow which is affected by the wall surfaces. Another factor is the extent of acceleration of the primary flow due to the existence of a jet stream. The height of the flow path in this experiment and the size of the air hole are close to the conditions of an actual burner. This indicates that the effect of the flow path height must also be considered in dealing with a burner. /20

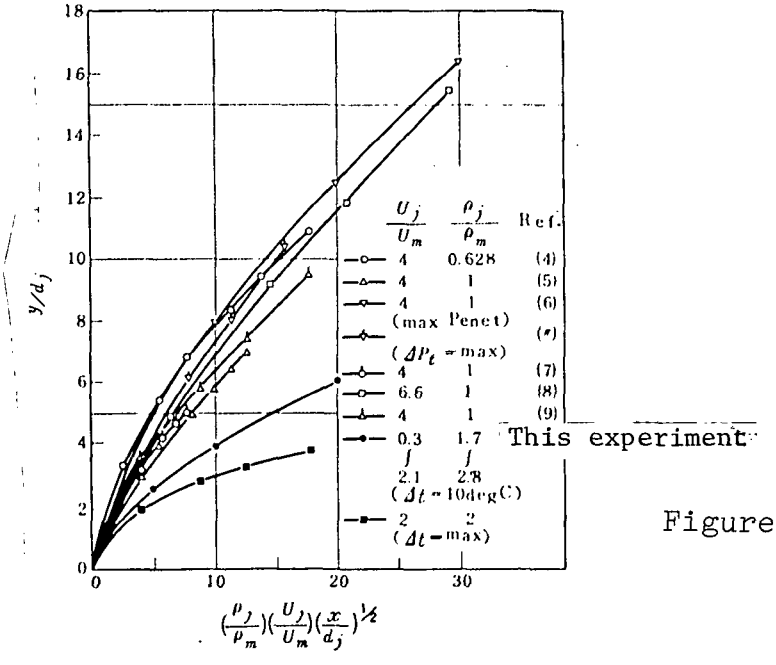

Figure 38. Jet stream path

TABLE 3. MIXTURE EXPERIMENTS OF JET STREAM FROM SINGLE ROUND HOLE PERPENDICULAR TO PRIMARY STREAM

Researcher (year)	Experiment method	Range of velocity ratio U_j/U_m	Diameter of jet stream hole d_j (mm)	Ratio of height of flow path to diameter of jet stream hole h/d_j	Literature
CALLAGHAN, RUGGERI, BOWDEN (1948 ~ 52)	Heated jet stream → normal temp. jet stream. For determination of the degree of penetration based on measurement temperature (Δt = 1 °F)	2 ~ 10	6.4 9.5 12.7 15.9	79.4 53.5 40 32	4 10 11
JORDINSON (1956)	Measurement of total pressure distribution within wind tunnel (ΔP_t = max)	4 ~ 8	12.7 25.4	120 60	5
CORDIER (1956)	Total pressure distribution (ΔP_t = max), using colorimetry in water tunnel (maximum penetration)	4 ~ 8	9.5 12.7	48 36	6
KEFFER, BAINE (1963)	Velocity distribution in thermic ray anemometer (ΔU = max)	2 ~ 10	9.5	246.5	7
PATRICK (1967)	Velocity and density within wind tunnel (ΔP_t = max)	6.6 ~	3.3 6.5 8.0 10.0	1,663 845 686 549	8
Endo, Nakamura (1970)	Total pressure distribution within wind tunnel (ΔP_t = max)	2.4 ~ 7.9	20	26	9
This experiment	Normal temp. jet stream → heated jet stream. For determination of degree of penetration based on temperature measurement (Δt = 10°C, maximum)	0.14 ~ 2.9	20	6.5	

Okamoto and Yagita [12] have conducted experiments on isothermal flow in measurement sections in which there is a wall only on a given side of the air hole, and the other sides are open. These results were compared with those of other research. The ratio involved selecting the abscissa as x/d_j. The jet stream path of the three open sides matched the other experimental results when $U_j/U_m = 4$. Under conditions in which the effect of the wall is believed to be great, $U_j/U_m = 8$, the penetration was shown to be somewhat greater than in other experiments.

5. Conclusion

In this report, the results of the series of three holes, long holes and two opposing round holes were exhibited from among the series of experiments on flow from air holes. Consolidated results on the single round hole prepared after the preceding report were also disclosed. The following conclusions were reached from the experimental results given.

(1) The flow rate coefficient of the air hole is indicated schematically as a function of the momentum ratio of the primary flow and the jet stream. As the momentum ratio increases, the flow rate coefficient gradually reaches a value of 0.8 to 0.9. When the momentum ratio is low, the coefficient assumes varying values based on the arrangement of the air holes and on the height of the guide tubes.

(2) The flow pattern of a series of three holes, of long holes and of two opposing round holes was indicated schematically. Variations were indicated based on the mode of combination and on the configuration of the air holes.

(3) Empirical formulas of the degree of penetration based on the distance for the maximum jet stream to be achieved were determined for the series of three holes and for long holes. In the case of two opposing round holes, the jet streams collided

when the jet stream velocity was high, and a low temperature section in the center of the flow path formed. The degree of penetration was lower than in the case of a single round hole.

(4) The path of the jet stream was determined from the line linking Δt = max of the center of the jet stream and from the isothermic line of Δt = 10 deg C in the periphery of the jet stream. The results were examined and compared with the results of a single round hole along with exhibition of an empirical formula.

(5) The degree of mixture exhibiting the extent of overall mixture of the jet stream and the primary stream was determined from temperature measurement. The empirical formula was exhibited for each air hole.

(6) The temperature distribution patterns within the jet stream exhibit similarities. The range of low temperature in the center of the jet stream was broader than the free cold jet stream. /21

(7) An empirical formula was exhibited for the path of Δt = max at the center of the jet stream of a single round hole. The results of the jet stream path compared with other experiments disclosed that the effects of flow path height must be considered with applying experimental results to burners.

In conducting these experiments, the authors were assisted by then students Koji Kurita, Yoshio Nagahara, Toshikatsu Asano, Takayoshi Nogami and Hirofumi Ishizaki of Tokai University and would like to express their appreciation to them.

REFERENCES

1. Kunio Suzuki, Tetsuro Ainami. On the flow from air holes of high load burners (I), National Aeronautics Laboratory Technical Memorandum TM-116 (1967).

2. Tetsuro Ainami, Masayuki Inoue. On the flow from air holes of high load burners (II), National Aeronautics Laboratory Technical Memorandum TR-227 (1970)

3. M. S. Uberoi and L. C. Garby. Effect of Density Gradients on an Air Jet, Physics of Fluids (1967), pp. S200-S202.

4. E. E. Callaghan and R. S. Ruggeri. Investigation of the penetration of an Air Jet Directed Perpendicularly to an Air Stream, NACA TN 1615 (1948)

5. R. Jordinson. Flow in a Jet Directed Normal to the Wind, Min. of Av. A.R.C.R. and M., No. 3074 (1956)

6. R. L. Gordier. Studies on Fluid Jets Discharging Normally into Moving Liquid, St. Anthony Falls Hydraulic Lab. Univ. of Minnesota, Tech. Paper No. 28, (Series B) (1959)

7. J. F. Keffer and W. D. Baines. The Round Turbulent Jet in a Cross Wind, J. Fluid Mech. (1963), pp. 481-497

8. M. A. Patrick. Experimental Investigation of Mixing and Flow in a Round Turbulent Jet Injected Perpendicularly into a Main Stream, J. Institute of Fuel (1967), pp. 425-432

9. Hiroshi Endo, Masayoshi Nakamura. Curvature of three dimensional turbulent jets in cross winds and development. National Aerospace Laboratory Technical Memoradum TR-216 (1970)

10. R. S. Ruggeri, E. E. Callaghan and D. T. Bowden. Penetration of Air Jets Issuing from Circular, Square and Elliptical Orifices Directed Perpendicularly to an Air Stream, NACA TN 2019 (1950)

11. E. E. Callaghan and R. S. Ruggeri. A General Correlation of Temperature Profiles of a Heated Air Jet Directed Perpendicularly to an Air Stream NACA TN 2466 (1951)

12. T. Okamoto and M. Yagita. The Effects of the Exit Velocity Profiles on the Flow of a Circular Jet Exhausting Normal to the Free Stream, Bulletin of the Tokyo Institute of Technology, No. 114 (1973)